Eye (2021) 35:996–1001
https://doi.org/10.1038/s41433-020-1017-7

The ROYAL COLLEGE of OPHTHALMOLOGISTS

ARTICLE

Simulation of the biomechanical effects induced by laser in situ keratomileusis (LASIK) for different levels of ablation in normal corneas

Rona Katzengold[1] · Amit Gefen[1] · Nir Sorkin[2,3] · David Smadja[4] · David Varssano[2]

Received: 9 December 2019 / Revised: 1 June 2020 / Accepted: 2 June 2020 / Published online: 16 June 2020

Abstract

Purpose To employ a finite element (FE) stress model to simulate laser in situ keratomileusis (LASIK) surgery and its biomechanical consequences.

Methods The basic geometrical model we used for the cornea was patient-specific on which we manually incorporated seven simulations: three simulations evaluating the effect of a 120, 140 and 180 μm flap (without ablation); three simulations evaluating ablation depths of 40, 80 and 120 μm (with a 120 μm flap); and one control model, without any simulated surgical intervention.

Results In all simulations, stress values were greatest in the centre of the cornea. Furthermore, when comparing the different treatments, stress values were highest in the cornea with the deepest ablation, and were lowest in the non-treated cornea. Specifically, peak effective stresses were 0.031, 0.028 and 0.025 MPa in 120, 80 and 40 μm ablation depths, respectively.

Conclusions In our model, the depth of tissue penetration using ablation or flap creation was correlated with tissue loads—the thinner the residual stromal bed is, the greater are the stresses occurring as a result of the same IOP.

Relevance We based our model geometry on patient specific scans, allowing for customisation of the treatment to the patient's corneal structure.

Introduction

Post-laser-assisted in situ keratomileusis (LASIK) ectasia, in which the cornea progressively becomes weaker after the surgery, is a major concern in refractive surgery as it degrades the vision and can severely affect the visual prognosis [1]. Therefore, a large portion of preoperative screening is focused on detecting refractive surgery candidates that may be at high risk for this complication [2–4]. Post LASIK ectasia is defined as a reduction in biomechanical integrity to below the threshold required to maintain corneal shape and curvature [5]. Therefore, the ability to simulate and predict preoperatively the biomechanical effects of LASIK on the cornea, so that excessive postoperative weakening is avoided, would be ideal in preoperative screening examination, in order to anticipate post-LASIK ectasia [6].

In a previous paper published by our group [7], a biomechanical model of a patient-specific cornea was developed by employing a realistic representation of the corneal geometry and anisotropic tissue mechanical properties. The aforementioned study included mathematical formulation for assessing patient-specific biomechanical properties of the human cornea as well as finite element (FE) analyses simulating the effects of different degrees of intraocular pressure (IOP) increase on the corneal structure. In that analysis, the model comprised of patient-specific corneal geometry as well as formulation for patient-specific corneal biomechanics.

In the present study, we employed the above model to simulate LASIK surgery and its biomechanical consequences,

✉ David Varssano
varssano@gmail.com

1 Department of Biomedical Engineering, Faculty of Engineering, Tel Aviv University, Tel Aviv, Israel

2 Department of Ophthalmology, Tel Aviv Medical Center, Sackler Faculty of Medicine, Tel Aviv University, Tel Aviv, Israel

3 Department of Ophthalmology and Vision Sciences, University of Toronto, Toronto, ON, Canada

4 Department of Ophthalmology, Shaare Zedek Medical Center, Jerusalem, Israel

to allow better understanding of the mechanical influence of LASIK treatment on the cornea and to determine the maximum tolerated magnitude of pressure-induced strains and stresses within the treatment zone.

Methods

The study was approved by the institutional review board of the Tel Aviv Medical Center and followed the tenets of the declaration of Helsinki.

Model and setting

The basic geometrical model we used for the cornea was a patient-specific model, which was developed in our group as described by Asher et al. [7]. Briefly, following informed consent the patient-specific corneal geometry was imaged using the GALILEI™ Dual Scheimpflug Analyser (Ziemer Group; Port, Switzerland). The geometrical data were imported into MATLAB (MathWorks, Natick, Massachusetts, United States) from two separate files, each containing one surface of the cornea (anterior and posterior) on an 8 mm diameter domain. The sampled points from both surfaces were assembled together and anatomically extrapolated to produce a point cloud file of the cornea-sclera on a 14 mm diameter domain. The result was converted into stereolithography (STL) format, a file format which approximates the surfaces of a solid model with triangles, using ADINA (ADINA Inc., Watertown, MA, USA) and loaded as such into the Simpleware finite element suit (Simpleware Ltd, Ver. 2012, Exeter, UK) [8]. The STL data were sampled with a 20 µm spaced grid and the resulting mask was partitioned into two separate parts; the cornea on an 11.89 mm domain (patient-specific white to white—WTW) with central thickness of 600 µm, and the sclera completing the domain up to 14 mm [7] (Fig. 1). In this study, we used the basic cornea model and manually incorporated a 40 µm epithelial layer [9].

Simulations

As a first step, we evaluated the biomechanical influence of flap creation alone (without ablation) by incorporating three models with varying flap thicknesses of 120, 140 and 180 µm. Then, for the LASIK treatment models, we simulated three scenarios with ablation depths of 40, 80 and 120 µm, which would roughly represent ablations for myopic corrections of 3, 6 and 9 D, according to Munnerlyn's law for an optical zone diameter of 6.5 mm [10]. Flap thickness in the treatment models was 120 µm with a flap diameter of 9 mm and a superior hinge (Fig. 1a, Table 1). Due to element size limitations, the treatment was formed as a disk of equal thickness (much like a photo-therapeutic keratectomy) and was not optical lens shaped. Creating a treatment disc, which approximates real myopic ablation would cause the elements' size to be too small and therefore the files would be too big for the computer to complete the simulations. The last model created was a control model of the cornea without any simulated surgical intervention. All model variants are summarised in Table 1.

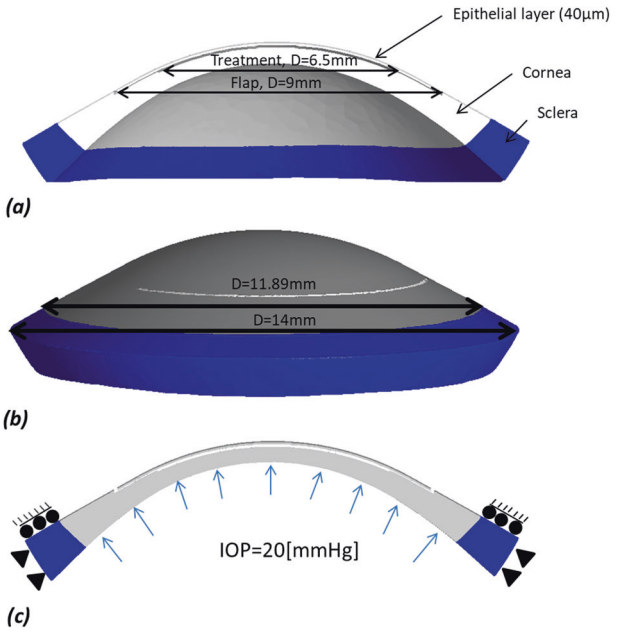

Fig. 1 Patient-specific corneal geometry, boundary conditions and loads. a A cross-sectional view of the cornea. Flap and treatment sections were added manually with diameter of 9 and 6.5 mm, respectively. **b** A 3D view of the model. The corneal domain is 11.89 mm (coloured in grey) and the sclera (coloured in blue) completes the domain up to 14 mm. **c** The model was fixed at the scleral circumference and the anterior sclera was constrained to sliding. IOP was set to 20 mmHg and was applied on the posterior surface.

Table 1 Summary of simulated treatments variants.

	Treatment	Ablation depth [µm]	Flap thickness [µm]
Case 1	120 µm flap	0	120
Case 2	140 µm flap	0	140
Case 3	180 µm flap	0	180
Case 4	40 µm ablation	40	120
Case 5	80 µm ablation	80	120
Case 6	120 µm ablation	120	120
Case 7	No treatment	0	0

Finite element modelling

The cornea tissue was assumed to behave as a third-order Ogden strain energy function (a hyperelastic material model

used to describe the non-linear stress–strain behaviour of complex materials such as biological tissue), based on patient-specific geometrical measurements, as described in Asher et al. [6]. The epithelial layer and sclera were modelled as linear elastic materials with modulus of elasticity of 0.57 kPa and 2.35 MPa, respectively [11, 12].

The boundary conditions were set as fixed along the rim of the sclera and only sliding was allowed on the anterior surface of the sclera. The interface between the epithelial layer and cornea and between the cornea and the sclera was set as 'tie' (no movement was allowed between two surfaces), to represent the structural linkage between these tissues. The interface between the posterior flap surface and the anterior stromal surface was set as frictional sliding with friction coefficient of 0.8 since this value allows the clinical situation we attempt to simulate; motion with large resistance between the flap and the stromal bed. The IOP was set as 20 mmHg for all simulations by setting a pressure boundary condition on the posterior surface of the cornea and sclera. This IOP is in addition to the IOP that existed when geometrical data were acquired (Fig. 1).

The models were all meshed using the Scan-IP module of Simpleware® [8]. Meshing the variants of all models was performed semi-automatically, with refinements around the flap, using the +FE free mesh creation algorithm. Using greater mesh densities did not provide a benefit in terms of numerical convergence or accuracy (resulted in <2% difference in stress data for denser meshes in preliminary analyses). Numbers of elements in all models varied between 1,341,374 and 1,883,779.

The FE simulations were all set up and pre-processed using PreView (Ver. 1.16.3, University of Utah, USA), analysed using the Pardiso linear solver of FEBio (Ver. 2.3.1) in structural mechanics mode, and post-processed using PostView (Ver. 1.9.0) [13].

A log file was created for the instantaneous curvature analysis, recording the nodal displacements (nodes of tetrahedrons forming the mesh) per each time step in the analysis until the full extent of deformation has been achieved.

Outcome measures

The cornea models were analysed for effective stress values, which can indicate future weakening of the cornea. Outcome measures included: (1) Distributions of effective stress values in corneal tissue. (2) Effective stress values through a vertical axis in the centre of the cornea. (3) Peak (maximal) effective stress values in the cornea. These outcome measures were compared between the different corneal treatment simulations detailed in Table 1.

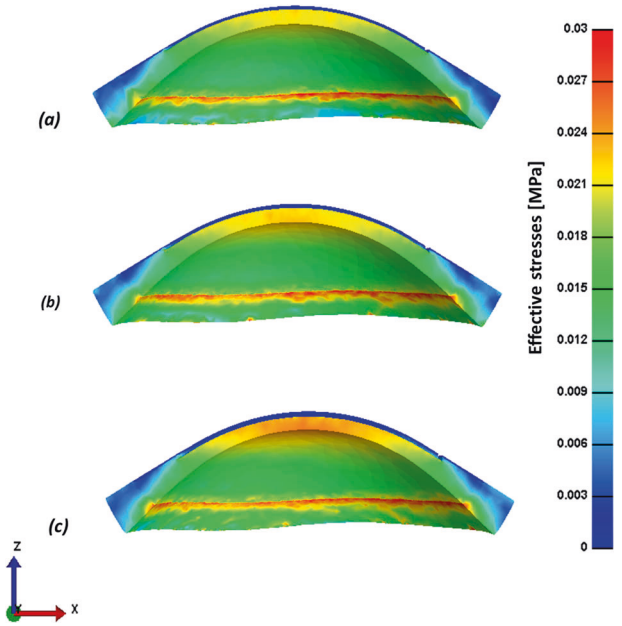

Fig. 2 Effective stress distributions after applying IOP of 20 mmHg: different flap thiknesses. A comparison of different flap section thicknesses: **a** 120, **b** 140 and **c** 180 µm flaps.

Results

Effective stress distributions, through a cross-sectional view of the corneas, for the different levels of flap thickness and of ablation depths simulated under 20 mmHg are presented in Figs. 2, 3, respectively. As expected, since the cornea is thinnest in its centre and thicker towards the limbus and sclera in a relatively symmetrical manner, stresses are indeed greatest in the centre (Figs. 2, 3). Flap thickness influenced stresses in the volume of the cornea under the flap. The thicker the flap was, the greater were the stresses induced by the applied IOP (Fig. 2). A finding which is common for all simulations is that stresses measured in the epithelial layer were lower than those measured in the cornea (Figs. 2, 3). In addition, Fig. 3 shows that stresses were greater in the treated corneas (Fig. 3a–d) compared with the non-treated cornea (Fig. 3e), and that they are greatest when treatment depth is greatest.

A plot of effective stress values along a vertical axis in the middle of the cornea shows a slight ascent of the stress values, with the highest values measured in the anterior part of the residual stromal bed (behind the flap/epithelial layer) (Fig. 4). A comparison of these plots between the different types of treatments also shows that stresses are highest in the cornea with the more significant treatment (120 µm) and are lowest in the non-treated cornea (Fig. 4b). Specifically, peak effective stresses were 0.031, 0.028 and 0.025 MPa in the 120, 80 and 40 µm treatments, respectively (Table 2). Figure 5 shows that average effective stresses in the centre of the cornea increase with elevation of ablation depth and

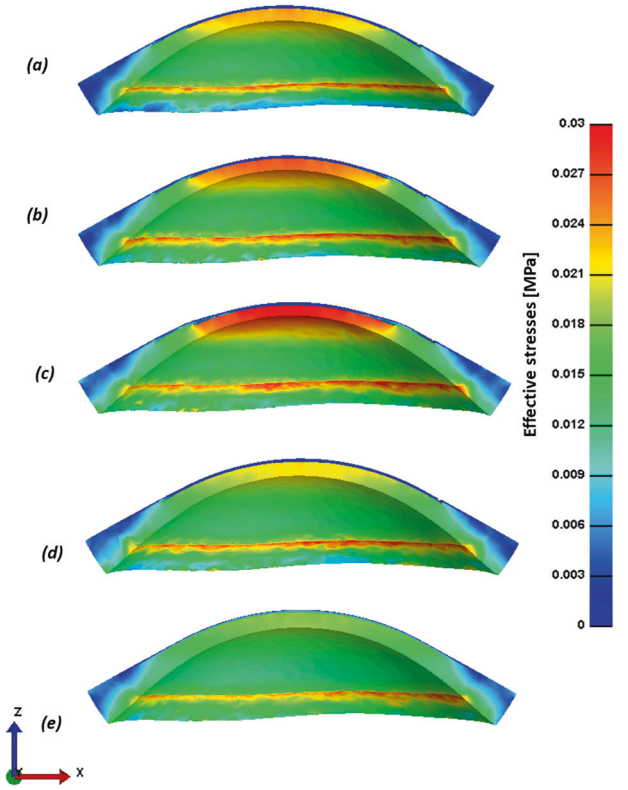

Fig. 3 Effective stress distributions after applying IOP of 20 mmHg: different ablation depths. A comparison of different LASIK ablation depths: **a** 40 **b** 80 and **c** 120 µm ablations. For validation, the LASIK procedures are also compared with **d** a cornea with only 120 µm flap section and to (e) a healthy, untreated cornea.

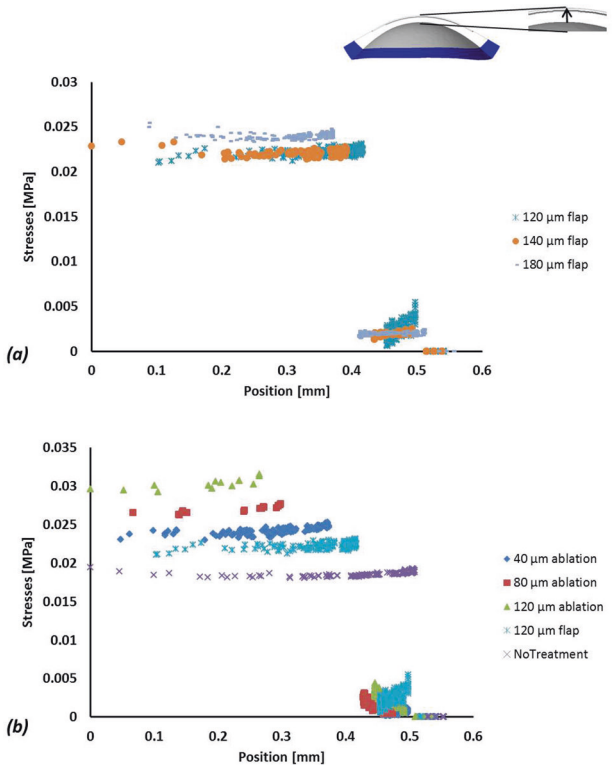

Fig. 4 A comparison of effective stresses [MPa] versus depth inside the central stroma. Depth is relative to the posterior corneal surface, as demonstrated in the top-right panel. Graph **a** is a comparison of different flap sections and graph **b** is a comparison of different LASIK procedures.

with elevation of flap depth in the range of treatments examined. The trendline formula for central corneal stress with change in flap thickness is: Stress $= (5 \times 10^{-5})$ Flap depth $+ 0.015$. The trendline formula for central corneal stress with change in ablation depth under a 120 µm flap is: Stress $= (9 \times 10^{-5})$ Ablation depth $+ 0.0088$.

Discussion

Several factors have been implicated in the development of post-LASIK ectasia. In this context, computational FE modelling would be helpful for predicting and comparing biomechanical efficacies of surgical techniques in corneal treatments and associated potential complications [7, 14, 15].

In our study, we have used computational FE modelling to evaluate the influence of LASIK surgery on the weakening of the cornea and its surrounding tissues. Stress values measured in the epithelium layer are much lower than the ones that were measured in the cornea itself, due to its relatively lower stiffness. This result agrees with previous knowledge that the epithelium layer does not have any involvement in corneal resistance and cohesive tensile strength [16]. As expected, stresses are greater in treated corneas (Figs. 3a–d, 4) compared with the non-treated cornea (Figs. 3e, 4), and they are the highest for deeper ablations. This is due to changes in effective thickness of the cornea: The thinnest the cornea, the greater are the stresses occurring as a result of the same IOP. Furthermore, the creation of a flap affects the stress values measured in the cornea post IOP implementation; stress values are lower in the only-flap cornea simulation compared with LASIK treated corneas, but are lowest in the non-treated cornea

Table 2 Element data of model variants.

	Treatment	Cornea	Epithelial layer	Sclera
Case 1	120 µm flap	920,392	569,144	140,383
Case 2	140 µm flap	925,596	599,680	218,960
Case 3	180 µm flap	955,658	596,845	215,793
Case 4	40 µm ablation	1,019,258	597,884	216,637
Case 5	80 µm ablation	948,090	597,296	216,739
Case 6	120 µm ablation	920,392	596,952	217,523
Case 7	No treatment	535,422	586,860	219,092

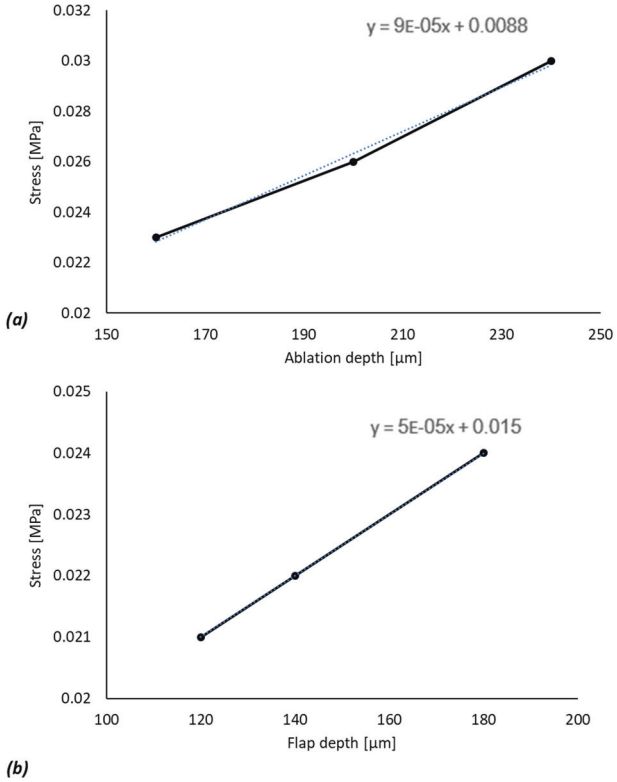

Fig. 5 Average effective stress [MPa] against intervention depths [µm]. The varying ablation depths with a fixed flap depth of 120 µm (**a**), and varying flap depth simulations and no ablation (**b**). Trend line formulas for each group are presented in the graph.

simulation (Figs. 2, 3, 4). It is interesting to see that when comparing stress distribution between the different flap thicknesses, the thicker the flap is, the greater are the stress values (Fig. 2). Although stress levels increased with the depth of intervention, the increase does not seem to be linear. The rate of stress increase appears to rise as the depth of intervention into the cornea increases. The initial stress increase in the flap-thickness change simulations appears linear. However, deeper intervention in the ablation-depth change simulations (with a 120 µm flap) produces higher stress values. When looking at the trendlines of both simulation groups (Fig. 5), we can see that the trendline slope of the ablation-change simulation group is nearly double (9/5-fold) that of the flap-thickness change group. The two trend lines intersect at a depth of 155 µm, and we can speculate that this would approximate the depth where linear stress increase changes its slope. One possible explanation for the rising rate of stress increase could be the different diameters of the flap (9.0 mm) and the ablation (6.5 mm). Another explanation could be that as the cornea thins, the same amount of tissue that is removed constitutes a higher percentage of the corneal thickness. For example, simplifying the calculations, when ablating 50 µm out of 500 µm stroma in a cornea, the relative force applied to every micron of the remaining stroma would increase 1.111-fold (500 µm/450 µm). When ablating the next 50 µm out of the remaining 450 µm stroma in that cornea, the relative force applied to every micron of the remaining stroma would now increase 1.125-fold (450 µm/400 µm). If we were to continue ablating on and on, then when ablating 50 µm out of the last 100 µm stroma of that cornea, the relative force applied to every micron of the remaining stroma would now increase twofold (100 µm/50 µm). This issue should be further studied and simulated.

Clearly, the cornea is weaker when its effective thickness is lower. The weaker the cornea is, the greater are the deformations induced by the same level of IOP, which causes a steepening of the central corneal structure (at the weakest part). Importantly, the central cornea is the weakest part since it is the area with the most ablated or severed lamellae. Sinha et al. [15] also investigated the influence of laser surgery on the cornea using finite element model methods. In their work, they compared between two vision correction laser procedures, LASIK and small-incision lenticule extraction, and presented stress distributions for both treatment types. However, their model geometry is based on average values and not on patient specific scans, which may have some limitations.

As with any modelling work, there are inherent limitations that need to be discussed. Although our model may provide useful clinical information, the simulations do not consider the variations in biomechanical properties throughout the corneal thickness (such as differences in biomechanical properties within the stroma at different depths as well as biomechanical properties of Bowman's layer) at this stage, although it is now well accepted that the anterior corneal stroma has greater corneal tensile strength than the posterior wall [15]. It may be beneficial to consider adding the stiffness gradient along the thickness of the cornea in order to provide a more complete representation of corneal biomechanics. However, the relevant experimental data are sparse and adding a stiffness gradient will highly complicate the computations. Another limitation is the incorporation of the treatment procedure. Our models are patient-specific; however, the 'virtual' treatments are not, we have manually added them and therefore they are not shaped as realistic ones. Nevertheless, we introduced the virtual ablation profiles to mimic real-world procedures using computer software (Scan-IP module of Simpleware®), under supervision of a cornea surgeon (DV) but not necessarily taking the full complexity of clinical considerations at the time of operation on an individual. Accordingly, the 'virtual' introduction of an ideal section somewhat compromises the specificity of our models, however, this is a practical way to methodologically and quantitatively predict the biomechanical outcomes of a treatment approach. Further validation of this model using

preoperative data of post LASIK ectasia patients, could help in obtaining the patient-specific biomechanical threshold to avoid ectasia. Following validation, this model, combined with clinical scoring systems, could improve preoperative detection of at-risk patients using both biomechanical and clinical data.

To conclude, we have developed a method and modelling framework, using computational FE-based techniques, to approximate the post-operative biomechanical behaviour of the cornea. This method has allowed us to mathematically model the stresses that the cornea is exposed to with corneal ablative surgery. Such a method, once clinically validated with whatever modifications may prove necessary, could eventually allow clinicians to more accurately plan surgeries and adjust their plan to increase the likelihood of avoiding post-operative ectasia.

Summary

What was known before

- Iatrogenic keratectasia can be induced by LASIK.
- Much effort is made to identify patients that may develop keratoectasia.
- There is no method to reliably predict if a specific eye would have post LASIK keratoectasia.

What this study adds

- Finite element modelling allowed us to see in advance the extra stress and strain induced on the cornea following LASIK.

Compliance with ethical standards

Conflict of interest The authors declare that they have no conflict of interest.

Publisher's note Springer Nature remains neutral with regard to jurisdictional claims in published maps and institutional affiliations.

References

1. Lam K, Rootman DB, Lichtinger A, Rootman DS. Post-LASIK ectasia treated with intrastromal corneal ring segments and corneal crosslinking. IGIT J Ophthalmol. 2013;19:1–8.
2. Santhiago MR, Smadja D, Gomes BF, Mello GR, Monteiro ML, Wilson SE, et al. Association between the percent tissue altered and post-laser in situ keratomileusis ectasia in eyes with normal preoperative topography. Am J Ophthalmol. 2014;158:87–95.
3. Tatar MG, Kantarci FA, Yildirim A, Uslu H, Colak HN, Goker H, et al. Risk factors in post-LASIK corneal ectasia. J Ophthalmol. 2014;2014:204191.
4. Said A, Hamade IH, Tabbara KF. Late onset corneal ectasia after LASIK surgery. Saudi J Ophthalmol. 2011;25:225–30.
5. Dawson DG, Randleman JB, Grossniklaus HE, O'Brien TP, Dubovy SR, Schmack I, et al. Corneal ectasia after excimer laser keratorefractive surgery: histopathology, ultrastructure, and pathophysiology. Ophthalmology. 2008;115:2181–91.
6. Yazici AT, Kara N, Yüksel K, Altinkaynak H, Baz O, Bozkurt E, et al. The biomechanical properties of the cornea in patients with systemic lupus erythematosus. Eye. 2011;25:1005–9.
7. Asher R, Gefen A, Moisseiev E, Varssano D. Etiology of keratoconus: proposed biomechanical pathogenesis. Silico Cell Tissue Sci. 2014a;1:3.
8. Simpleware® Ltd. ScanIP, +FE, +NURBS and +CAD Reference Guide ver. 5.1, 2012. http://www.simpleware.com/software/.
9. Reinstein DZ, Archer TJ, Gobbe M, Silverman RH, Coleman DJ. Epithelial thickness in the normal cornea: three-dimensional display with very high frequency ultrasound. J Refract Surg. 2008;24:571–81.
10. Munnerlyn CR, Koons SJ, Marshall J. Photorefractive keratectomy: a technique for laser refractive surgery. J Cataract Refract Surg. 1988;14:46–52.
11. Thomasy SM, Raghunathan VK, Winkler M, Reilly CM, Sadeli AR, Russell P, et al. Elastic modulus and collagen organization of the rabbit cornea: epithelium to endothelium. Acta Biomater. 2013;10:785–91.
12. Kniestedt C, Punjabi O, Lin S, Stamper RL. Tonometry through the ages. Surv Ophthalmol. 2008;53:568–91.
13. Maas SA, Ellis BJ, Ateshian GA, Weiss JA. FEBio: finite elements for biomechanics. J Biomech Eng. 2012;134:5–11.
14. Asher R, Gefen A, Moisseiev E, Varssano D. An analytical approach to corneal mechanics for determining practical, clinically-meaningful patient-specific tissue mechanical properties in the rehabilitation of vision. Ann Biomed Eng. 2014b; 43:274–86.
15. Sinha Roy A, Dupps WJ Jr, Roberts CJ. Comparison of biomechanical effects of small-incision lenticule extraction and laser in situ keratomileusis: finite-element analysis. J Cataract Refract Surg. 2014;40:971–80.
16. Dupps WJ Jr, Wilson SE. Biomechanics and wound healing in the cornea. Exp Eye Res. 2006;83:709–20.